Periodica Polytechnica Chemical Engineering, 68(4), pp. 552–560, 2024

Efficient Catalytic Hydrocracking of Crude Palm Oil Over EDTA Template-assisted SiO_2-Al_2O_3/NiMo Catalysts

Zainal Fanani[1], Wan Ryan Asri[2], Betty Dwiyanti[1], Nino Rinaldi[3], Roni Maryana[3], Muhammad Al Muttaqii[3], Fahma Riyanti[1], Ady Mara[1], Rahadian Zainul[4], Hasanudin Hasanudin[1*]

[1] Department of Chemistry, Faculty of Mathematics and Natural Science, Universitas Sriwijaya, Jl. Palembang-Prabumulih Km. 35., 30662 Indralaya, Sumatra Selatan, Indonesia
[2] Chemistry Department, King Fahd University of Petroleum and Minerals, 31261 Dhahran, Saudi Arabia
[3] Research Center for Chemistry, Indonesian Institute of Sciences, Building 452 Kawasan PUSPIPTEK, Serpong, 15314 Tangerang Selatan, Banten, Indonesia
[4] Department of Chemistry, Faculty of Mathematics and Natural Science, Universitas Negeri Padang, Jl. Prof. Dr. Hamka 1., 25171 Padang, Indonesia
* Corresponding author, e-mail: hasanudin@mipa.unsri.ac.id

Received: 22 April 2024, Accepted: 21 August 2024, Published online: 10 October 2024

Abstract

The development of hydrocracking catalysts for crude palm oil (CPO) is a challenging process due to its limited textural or pore accessibility and low acidity properties. Therefore, this study aims to develop a series of SiO_2-Al_2O_3-x/NiMo catalysts using different Al mass (x = 5, 10, 25 g) assisted with EDTA to enhance their physicochemical properties. During the procedures, bimetallic NiMo species were dispersed into SiO_2-Al_2O_3-x using the wet impregnation method. The structural, textural, surface morphology, particle size distribution, and acidity properties of the products were then assessed. Catalytic activity of catalysts on hydrocracking of CPO was evaluated at 350 °C for 2 h, H_2 gas pressure of 20 bar, and mixed at 1500 rpm. The results showed that increasing Al mass caused an increment in the total acidity, acid site density, and surface area of SiO_2-Al_2O_3-x. In addition, SiO_2-Al_2O_3-25 provided better support properties, allowing preferable NiMo dispersion. Hydrocracking assessment showed that CPO conversion was increased at higher Al mass, producing the highest bio-aviation and biogasoline fractions yield. Based on these results, SiO_2-Al_2O_3-x/NiMo successfully enhanced CPO conversion of unloaded SiO_2-Al_2O_3-x, as well as increased the yield of bio-aviation and biogasoline fractions.

Keywords

catalytic hydrocracking, NiMo, SiO_2-Al_2O_3, crude palm oil, bimetallic catalyst

1 Introduction

The growing need for energy and the decreasing supply of conventional fuel are major factors facilitating the development of cleaner and sustainable energy [1]. Consequently, biofuel production from renewable resources has received significant attention in recent years. This is primarily due to its ability to compensate for the decreasing supply of fossil fuels, lower carbon footprint, as well as enhance economic growth and sustainability [2]. Biofuel production is often carried out using crude palm oil (CPO) and its derivatives as biomass due to their low cost and high output per hectare relative to other vegetable oils in Southeast Asia [3]. At present, the most prevalent method for this process is triglyceride hydroprocessing, which comprises the use of high temperature and pressure with different catalysts [4]. Triglyceride hydroprocessing typically consists of several steps, including hydrogenation and cracking. Hydrogenation often begins by transforming unsaturated fatty acids into saturated acids, followed by breaking fatty acids into short-chain hydrocarbons through complex chemical processes, such as hydrodeoxygenation, decarboxylation, and decarboxylation [5]. Meanwhile, hydrocracking converts CPO into hydrocarbons, which is an alternate method for producing low S and N hydrocarbons.

Several studies have shown that the types of catalysts significantly impact the efficiency of hydrocracking. Various types, such as HZSM-5 and HY zeolites [6], Zn-Mo/HZSM-5 [7], Ni/zeolite [8], ZSM5 zeolite [9], Mo/SiO_2 [10], SiO_2/ZrN [11], NiO-CdO/biochar [12], Ni-Mo/alumina [13], Ni–W/SiO_2–Al_2O_3 [14], and NiMoW-ZSM-5/MCM-41 [15], have been used for vegetable

Cite this article as: Fanani, Z., Asri, W. R., Dwiyanti, B., Rinaldi, N., Maryana, R., Al Muttaqii, M., Riyanti, F., Mara, A., Zainul, R., Hasanudin, H. "Efficient Catalytic Hydrocracking of Crude Palm Oil Over EDTA Template-assisted SiO_2-Al_2O_3/NiMo Catalysts", Periodica Polytechnica Chemical Engineering, 68(4), pp. 552–560, 2024. https://doi.org/10.3311/PPch.37159

oil-based hydrocracking. Despite the potential, noble monometal-based catalysts are less effective due to the ease of deactivation by sintering active metal species and coke deposits, leading to unstable and poor catalytic activity [16]. This has led to the use of bifunctional catalysts, which often comprise both metal and acid sites. The materials also have hydrogenation sites that can supply hydrogen for hydrogenation processes and surface hydrogenolysis [17]. Although noble metal-based catalysts perform better in hydrocracking, their high costs can diminish economic viability, necessitating the consideration of alternatives [16]. Among the transition metals, Ni and Mo are commonly used in hydrocracking reactions and have shown exceptional catalytic activity [18].

Various types of catalysts using NiMo as active metals have been prepared with different supports [19–24]. In this context, alumina and silica are the most frequently used mesoporous oxide supports due to their tunable acidity and excellent stability [25, 26]. SiO_2-Al_2O_3 mixed oxides are prominent supports that offer various benefits during hydrocracking process. This material has adequate pore diameter to promote metal deposition and pore diffusion, optimal active metal dispersion, and appropriate acidity to break down larger molecules while reducing coke formation. SiO_2-Al_2O_3 oxides can also be modified to provide the desired acidity and textural characteristics [27, 28]. According to a previous study [11], the use of ethylenediaminetetraacetic acid (EDTA) as a template method successfully enhanced the acidity, metal dispersion, and textural features of SiO_2/Zr-based catalysts, providing better catalytic hydrocracking performance. Therefore, this study aims to develop mesoporous SiO_2-Al_2O_3/NiMo catalysts with different Al mass using EDTA as a template agent to enhance their physicochemical properties. Dispersing NiMo into SiO_2-Al_2O_3 supports is expected to enhance the intrinsic performance of CPO hydrocracking towards high conversion.

2 Materials and methods

2.1 Preparation of SiO_2-Al_2O_3

SiO_2-Al_2O_3 was prepared using the sol-gel method with different Al mass (5, 10, 25 g with Si:Al ratio 1:0.02, 1:0.05, 1:0.15, respectively) and assisted with EDTA as a template. All chemicals for catalyst preparation were purchased from Sigma-Aldrich and used without further purification. A total of 25 g of disodium salt of EDTA ($C_{10}H_{14}N_2Na_2O_8{\cdot}2H_2O$, 99.0–101.0% purity) was dissolved in demineralized water (500 mL) and stirred, thus forming 5% of EDTA solution. Subsequently, 5 g of aluminum nitrate nonahydrate salts ($Al(NO_3)_3{\cdot}9H_2O$, ≥98.5% purity) were dissolved in 100 mL of as-prepared EDTA solution and stirred at room temperature, and were later mixed with 100 mL of tetraethyl orthosilicate ($Si(OC_2H_5)_4$, ≥99.0%) and 200 mL of ethanol (CH_3OH, ≥99.5 purity) and stirred for 15 min at room temperature. Furthermore, the ammonia solution (NH_4OH, 25% purity) was gradually dripped into the latter solution until it became a gel, which was agitated for 30 min and subsequently stirred and heated up to 50 °C until forming a paste. The paste was dried at 100 °C for 24 h and calcined at 750 °C for 6 h. Its powder (120 mesh) was denoted as SiO_2-Al_2O_3-5. Further catalysts with different Al mass (10 and 25 g) was prepared with the same procedures and were denoted as SiO_2-Al_2O_3-10 and SiO_2-Al_2O_3-25, respectively.

2.2 Preparation of SiO_2-Al_2O_3/NiMo

SiO_2-Al_2O_3/NiMo was prepared using the wet-impregnation method. Typically, 5.06 g of nickel(II) chloride hexahydrate salt ($NiCl_2{\cdot}6H_2O$, 99.9% purity) was dissolved in 100 mL of demineralized water and stirred at room temperature. A total of 5.26 g of ammonium molybdate ($(NH_4)_2MoO_4$, purity 99.98%) was dissolved in 100 mL of demineralized water and mixed with the latter solution, forming NiMo precursors solution (molar ratio = 1:1). Furthermore, 25 g of SiO_2-Al_2O_3 was dispersed in the NiMo solution and stirred, gradually increasing the temperature to 80 °C until forming a paste, which was dried in the oven at 100–110 °C, calcined at 750 °C for 6 h, and at 350 °C for 2 h. The powder was denoted as SiO_2-Al_2O_3-x/NiMo, where x was the mass of Al.

2.3 Hydrocracking of CPO

In this procedure, 0.6 g of SiO_2-Al_2O_3-x and SiO_2-Al_2O_3-x/NiMo series catalysts and 20 g of CPO were used for hydrocracking and before hydrocracking, the reactor was purged 3 times with H_2 gas (20 bar). Hydrocracking was conducted at 350 °C for 2 h uder stirring with 1500 rpm. The liquid product was analyzed by the GC-MS. The triglycerides were denoted as TGs, whereas the biofuel yield (Y_x) and conversion (C_x) were calculated according to Eqs. ((1)–(2)):

$$Y_x = \frac{\%\ \text{area of biofuel in GC-MS}}{\text{TGs in reactant} - \text{TGs in product}} \times 100\%, \quad (1)$$

$$C_x = \frac{\text{TGs in reactant} - \text{TGs in product}}{\text{TGs in reactant}} \times 100\%. \quad (2)$$

2.4 Characterization of catalysts

Powder X-ray diffraction (XRD, Rigaku SmartLab) was used to analyze the phase structure of the catalysts, and FTIR spectrophotometer (Bruker Tensor II) was used to evaluate the functional groups of the catalysts. SEM-EDX mapping (Hitachi SU3500) was used to capture the surface morphology of the catalysts and their elemental constituents. The average particle size and its distribution were calculated on a micro-scale using a particle size analyzer (Horiba LA-960). Furthermore, the N_2 adsorption-desorption was recorded by a surface area analyzer (TriStar II 3020 , Micromeritics). The sample (0.3 g) was degassed at 300 °C for 3 h, with bath temperature of −195.85 °C and equilibration Interval of 5 s. The weight of the degassed sample was utilized in calculations.

The surface area was calculated using the multi-point Brunauer–Emmett–Teller method (BET), while the pore features were extracted using Barrett-Joyner-Halenda (BJH) method. The total acidity was measured using an NH_3-TPD (AutoChem II 2920, Micromeritics). The sample was degassed at 350 °C for 1 h and flowed with He gas. Subsequently, the temperature was increased gradually up to 500 °C for 30 min.

3 Results and discussion

3.1 Catalyst characterization

The XRD diffractograms of SiO_2-Al_2O_3-x and SiO_2-Al_2O_3-x/NiMo where x is the mass of Al (5, 10, 25 g) were presented in Fig. 1. The parent SiO_2-Al_2O_3-5 showed a wide diffraction peak at 2θ ca. 21°, suggesting the formation of amorphous silica structure [29]. The diffraction peaks appeared at 2θ = 27.46°, 31.17°, 35.85°, and 46.82°, confirming the γ-Al_2O_3 phase [30]. The broadened peak (2θ = 21°) upon higher Al mass (SiO_2-Al_2O_3-10 and SiO_2-Al_2O_3-25) showed a robust interaction between SiO_2 and Al_2O_3 [31]. The intensity of the γ-Al_2O_3 phase in SiO_2-Al_2O_3-10 significantly decreased and tended to disappear in SiO_2-Al_2O_3-25, implying that higher mass of Al decreased the crystallinity and promoted the formation of amorphous SiO_2-Al_2O_3 support. The SiO_2-Al_2O_3-5/NiMo catalyst exhibited a diffraction peak at 2θ 14.27°, 23.98°, 25.32°, 28.24°, 32.60°, and 48.32° corresponding to the presence of crystalline MoO_3 [32]. The monoclinic phase of the nickel molybdenum could be confirmed by the diffraction peaks at 2θ 25.97°, 26.77°, 27.4°, and 32.87° [33], while the diffraction peaks at 2θ 38.69°, 43.85°, and 61.75° were attributed to the nickel oxide phase [34]. The intensity of sharp peaks of metallic phases was much higher in the order of SiO_2-Al_2O_3-5/NiMo > SiO_2-Al_2O_3-10/NiMo > SiO_2-Al_2O_3-25/NiMo catalysts, which showed the presence of larger NiMo crystallite and poor dispersion in the support [35]. This result suggested that SiO_2-Al_2O_3-25 promoted better the bimetal dispersion than its counterparts. However, the diffraction intensity of silica (SiO_2-Al_2O_3-5/NiMo) increased upon NiMo loading owing to the interaction of the bimetallic species with the silica, which influenced the regularity of the SiO_2-Al_2O_3 framework.

Fig. 2 presented FTIR spectra of SiO_2-Al_2O_3-x and SiO_2-Al_2O_3-x/NiMo. The absorption bands at 805 cm^{-1} and 1066–1198 cm^{-1} in SiO_2-Al_2O_3-5 corresponded to the linkage vibration of Si–O–Al and the stretching vibration of Si–O–Si of the condensed silica-alumina framework formation, respectively [11, 36], and indeed had similar absorption bands characteristics to its counterparts. However, the shift upon higher Al mass in the silica bond

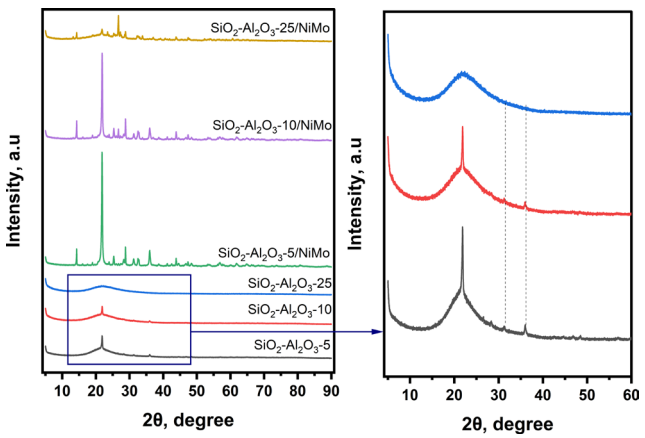

Fig. 1 XRD diffractograms of parent SiO_2-Al_2O_3 and SiO_2-Al_2O_3/NiMo catalysts with different Al masses

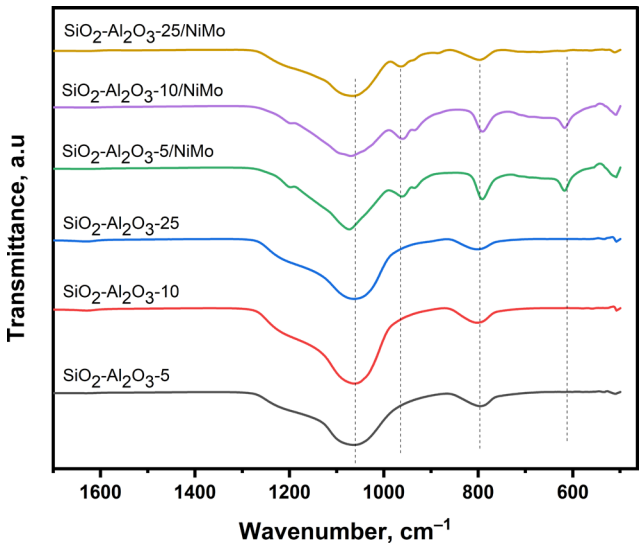

Fig. 2 FTIR spectra of parent SiO_2-Al_2O_3 and SiO_2-Al_2O_3/NiMo catalysts with different Al masses

(SiO_2-Al_2O_3-10 and SiO_2-Al_2O_3-25) presumably showed the increase of Si–O–Al hetero-linkages population in catalysts [37]. The absorption bands at 620–703 cm^{-1} in SiO_2-Al_2O_3-5/NiMo were ascribed to the Mo–O–Mo and Mo=O vibrations [22], while the absorption bands at 932–962 cm^{-1} were attributed to the Ni-O vibration. Similar absorption bands were also observed in SiO_2-Al_2O_3-10/NiMo with no appreciable changes. These absorption bands of the metals, however, tended to diminish in SiO_2-Al_2O_3-25/NiMo, suggesting a better interaction between the bimetallic species and the support, which was consistent with the XRD results. Moreover, the Si–O–Al absorption band in SiO_2-Al_2O_3-x/NiMo were slightly shifted to lower wavenumbers (ca. 795 cm^{-1}) and had higher intensity with respect to the parent catalysts, suggesting that the bimetalic species were incorporated into the framework of catalysts support [29].

Fig. 3 showed the SEM micrographs of unloaded SiO_2-Al_2O_3-x and SiO_2-Al_2O_3-x/NiMo. SiO_2-Al_2O_3-5 (Fig. 3 (a)) exhibited aggregated particles with irregular shapes, suggesting an amorphous nature [38]. Similar surface morphology features were also noticed in both $SiO_2Al_2O_3$-10 and $SiO_2Al_2O_3$-25 (Fig. 3 (b)–(c)). A change in surface morphology features was observed upon NiMo loading (Fig. 3 (d)–(f)), showing that changing the Al mass in the support could affect the surface morphology of the SiO_2-Al_2O_3-x/NiMo catalysts. Different Al mass in the support presumably reorganizes the arrangement of the particles within the surface, hence resulting in different morphologies upon NiMo loading.

Fig. 4 presented the EDX mapping of SiO_2-Al_2O_3-x and SiO_2-Al_2O_3-x/NiMo. SiO_2-SiO_2-Al_2O_3-5 (Fig. 4 (a)) showed Si and Al elements, confirming the formation of SiO_2-Al_2O_3, which was similar to SiO_2-Al_2O_3-10 and SiO_2-Al_2O_3-25 (Fig. 4 (b)–(c)) with increasing Al elements intensity upon higher Al mass. Ni and Mo element with homogenous distribution

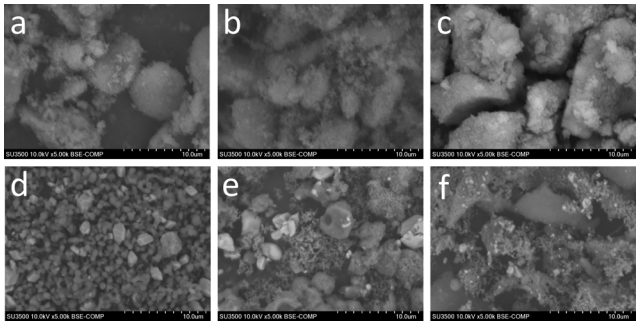

Fig. 3 SEM micrographs of (a) SiO_2-Al_2O_3-5; (b) SiO_2-Al_2O_3-10; (c) SiO_2-Al_2O_3-25; (d) SiO_2-Al_2O_3-5/NiMo; (e) SiO_2-Al_2O_3-5/NiMo; (f) SiO_2-Al_2O_3-5/NiMo

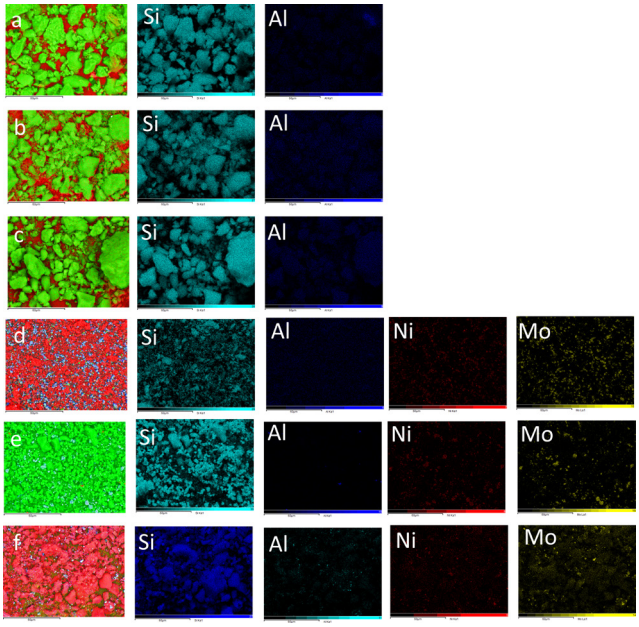

Fig. 4 SEM-EDX mapping of (a) SiO_2-Al_2O_3-5; (b) SiO_2-Al_2O_3-10; (c) SiO_2-Al_2O_3-25; (d) SiO_2-Al_2O_3-5/NiMo; (e) SiO_2-Al_2O_3-5/NiMo; (f) SiO_2-Al_2O_3-5/NiMo

appeared in SiO_2-Al_2O_3-x/NiMo (Fig. 4 (d)–(f)), showing that the NiMo species were successfully loaded onto the support. Fig. 4 showed that SiO_2-Al_2O_3-25/NiMo had more profound Ni and Mo intensity compared to its counterparts, suggesting an enhancement in the bimetal dispersion, corroborating the XRD and FTIR results.

The particle size distribution of SiO_2-Al_2O_3-x and SiO_2-Al_2O_3-x/NiMo was presented in Fig. 5, while the average particle size of catalysts was shown in Table 1. SiO_2-Al_2O_3-5 had a narrow particle size distribution with an average particle size of 5.63 ± 0.02 µm. This size

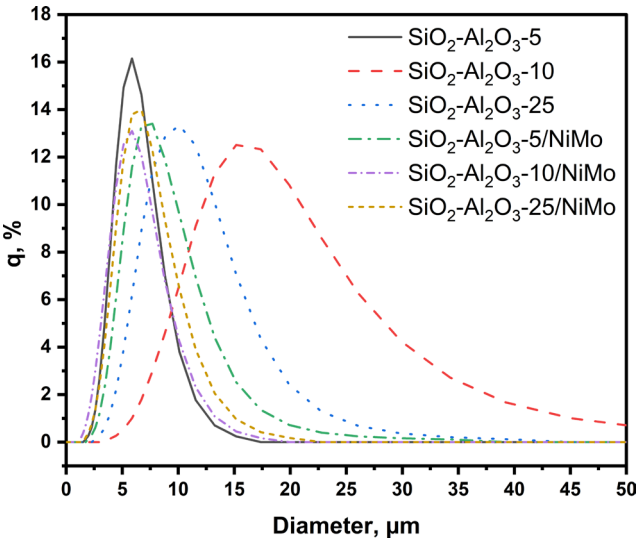

Fig. 5 The particle size distribution of SiO_2-Al_2O_3-x and SiO_2-Al_2O_3-x/NiMo catalysts

Table 1 The average particle size of SiO_2-Al_2O_3-x and of SiO_2-Al_2O_3-x/NiMo catalysts

Catalysts	Average particle size (μm)
SiO_2-Al_2O_3-5	5.63 ± 0.02
SiO_2-Al_2O_3-10	16.88 ± 0.06
SiO_2-Al_2O_3-25	9.78 ± 0.02
SiO_2-Al_2O_3-5/NiMo	7.48 ± 0.02
SiO_2-Al_2O_3-10/NiMo	5.45 ± 0.02
SiO_2-Al_2O_3-25/NiMo	6.26 ± 0.02

distribution became wider with increasing average particle size 16.88 ± 0.06 μm in SiO_2-Al_2O_3-10, suggesting a non-uniform particle size distribution. The particle size distribution tended to narrow upon higher Al mass (SiO_2-Al_2O_3-25) and to decrease its average particle size to 9.78 ± 0.02 μm. SiO_2-Al_2O_3-5/NiMo showed a higher average particle size (7.48 ± 0.02 μm) that slightly shifted towards higher particle diameter distribution for its parent catalysts, presumably owing to NiMo agglomeration. Meanwhile, SiO_2-Al_2O_3-10/NiMo and SiO_2-Al_2O_3-25/NiMo had narrow particle size distribution and a decrease in the average particle size (5.45 ± 0.02 and 6.26 ± 0.02 μm, respectively) compared to unloaded SiO_2-Al_2O_3, showing that increasing the Al weights prominently promoted better homogeneity of the particles hence providing good dispersion.

Fig. 6 showed the N_2 adsorption-desorption of isotherms SiO_2-Al_2O_3-x and SiO_2-Al_2O_3-x/NiMo. However, it appeared that all catalysts possessed type IV isotherm, showing mesoporous materials [39]. The presence of mesopores allowed an efficient movement of large molecules through the pores. The steep capillary condensation in the

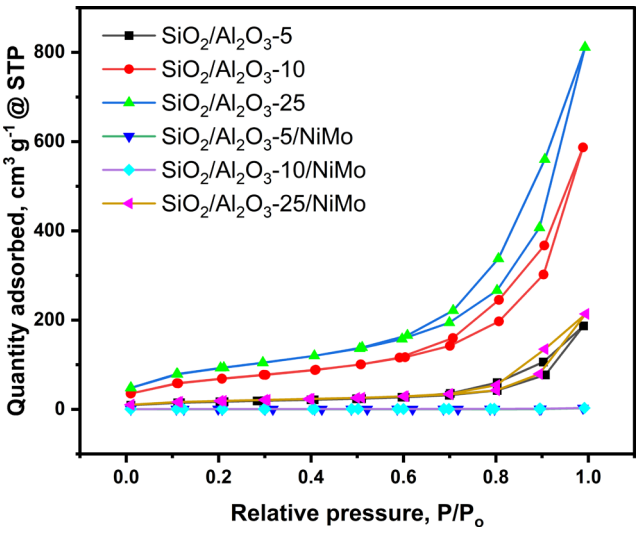

Fig. 6 N_2 adsorption-desorption of SiO_2-Al_2O_3-x and SiO_2-Al_2O_3-x/NiMo with different Al mass

relative pressure P/P_0 range of 0.65–0.85 was attributed to the non-uniform pore sizes and shapes [40].

Table 2 showed the BET surface area, pore volume, and the average pore diameter (which was calculated with the BJH method) of prepared catalysts. In addition, it could be seen that SiO_2-Al_2O_3-10 had a higher surface area than SiO_2-Al_2O_3-5 as well as pore volume and tended to increase upon higher weights of Al. This result could be attributed to the pore enlargement by Si-O-Al bonding [41]. However, upon NiMo loading, the surface area tended to decrease significantly in both SiO_2-Al_2O_3-5/NiMo and SiO_2-Al_2O_3-10/NiMo. This happened presumably owing to the partial occupation or blockage of the pore space in the support of the active metal phase [42, 43]. SiO_2-Al_2O_3-25/NiMo possessed the highest surface area than its counterpart and increased pore diameter for the unloaded SiO_2-Al_2O_3-25. The reason presumably could be due to changes in the electrostatic field in the pores of the support as the Al mass increases, which could cause electrostatic equilibrium in the pore supports, leading to an increase in pore diameter.

The total acidity of SiO_2-Al_2O_3-x and SiO_2-Al_2O_3-x/NiMo catalysts measured by NH_3-TPD was presented in Table 3 and the total acidity of unloaded SiO_2-Al_2O_3-x showed no appreciable change (~0.53 mmol NH_3 g^{-1} cat.) with increasing Al mass. The total acidity value

Table 2 The textural features of SiO_2-Al_2O_3-x and SiO_2-Al_2O_3-x/NiMo catalysts

Catalysts	BET surface area (m^2 g^{-1})	Pore volume (cm^3 g^{-1})	Average pore diameter (nm)
SiO_2-Al_2O_3-5	59	0.29	19.56
SiO_2-Al_2O_3-10	240	0.91	15.07
SiO_2-Al_2O_3-25	326	1.26	15.38
SiO_2-Al_2O_3-5/NiMo	2	0.004	8.66
SiO_2-Al_2O_3-10/NiMo	2	0.004	7.93
SiO_2-Al_2O_3-25/NiMo	64	0.33	20.38

Table 3 Total acidity of SiO_2-Al_2O_3-x and SiO_2-Al_2O_3-x/NiMo catalysts measured by NH_3-TPD

Catalysts	Total acidity (mmol NH_3 g^{-1} cat.)
SiO_2-Al_2O_3-5	0.54
SiO_2-Al_2O_3-10	0.53
SiO_2-Al_2O_3-25	1.07
SiO_2-Al_2O_3-5/NiMo	0.15
SiO_2-Al_2O_3-10/NiMo	0.20
SiO_2-Al_2O_3-25/NiMo	0.46

was predominantly driven by Lewis and Bronsted acid sites from silica and alumina, which tended to double upon higher Al mass (SiO_2-Al_2O_3-25) up to 1.07 mmol NH_3 g^{-1} cat. due to the enhancement of Al^{3+} Lewis acid sites. Meanwhile, a decrease in total acidity was noticed in SiO_2-Al_2O_3-x upon NiMo loading. This result was presumably due to the aggloeration of the NiMo species, which led to the blocking of the alumina-silica acidic sites [44]. Compared to its counterparts, the total acidity increased in the order of SiO_2-Al_2O_3-5/NiMo > SiO_2-Al_2O_3-10/NiMo > SiO_2-Al_2O_3-25/NiMo. However, this seemed to have a linear correlation with the surface area, suggesting that a high surface area could lead to high total acidity.

Fig. 7 showed NH_3-TPD profiles of unloaded SiO_2-Al_2O_3-x and SiO_2-Al_2O_3-x/NiMo with different Al mass. The desorption peaks at < 200 °C, corresponded to weak acidic sites, while the desorption peaks at 200–300 °C and > 300 °C showed the presence of medium and strong acidic sites, respectively [20]. SiO_2-Al_2O_3-5 had only strong acidic sites, while SiO_2-Al_2O_3-10 had both weak and strong acidic sites. The desorption peak intensity tended to increase pronouncedly upon higher Al mass (SiO_2-Al_2O_3-25), suggesting that increasing the Al mass led to an increase in the density of acidic and formed weak acidic sites. Both SiO_2-Al_2O_3-5/NiMo and SiO_2-Al_2O_3-10/NiMo had only strong acidic sites, but the latter had lower acid density. Moreover, SiO_2-Al_2O_3-25/NiMo had weak and strong acidic sites with higher density, showing better acidity strength compared to its counterparts.

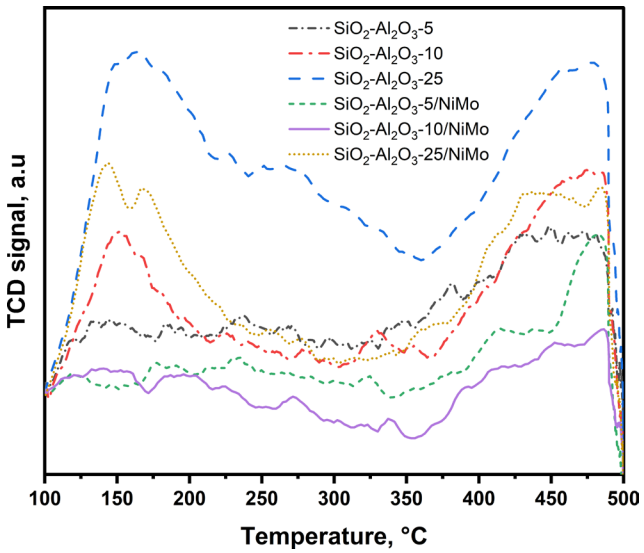

Fig. 7 NH_3-TPD profiles of SiO_2-Al_2O_3-x and SiO_2-Al_2O_3-x/NiMo with different Al mass

3.2 Catalytic performance in CPO hydrocracking

Table 4 shows the catalytic performance of SiO_2-Al_2O_3-x and SiO_2-Al_2O_3-x/NiM in terms of CPO conversion and biofuel yield. Additionally, it could be seen that SiO_2-Al_2O_3-5 had the lowest CPO conversion (75.78%) and tended to rise to 84.47% upon introducing 10 g Al on the support (SiO_2-Al_2O_3-10). The highest CPO conversion up to 91.20% was achieved by SiO_2-Al_2O_3-25, showing that increasing Al mass promoted higher CPO conversion owing to the weak-strong acidic sites derived from Si–(OH)–Al. It was reported that hydrocracking performance increased with the increase in the acidity of the catalyst [45]. Upon NiMo loading, SiO_2/Al_2O_3-5 had higher CPO conversion (92.99%) than its parent catalyst, presumably due to the moderately dispersed active metal within the pores of the catalyst, hence increasing its catalytic activity. Similarly, SiO_2/Al_2O_3-10 showed higher CPO conversion (91.34%) as well as SiO_2/Al_2O_3-25/NiMo (91.73%), suggesting a synergetic effect between the former acidic sites from alumina-silica and the dispersed NiMo species onto the support hence enhancing the CPO conversion. Although no appreciable change in the CPO conversion (~91–92%) was noticed in the case of the NiMo catalyst analogues, however, it possessed different catalytic activity in terms of biofuel yields. SiO_2-Al_2O_3-5 exhibited predominant bio-aviation (34.26%), followed by biodiesel (2.28%), and had the lowest biogasoline yields (2.28%). The high bio-aviation yield was attributed to the mesoporous structure that provided better diffusion and accessibility between the CPO and acidic sites, hence selectively forming C_{10}-C_{14} carbons. Unloaded SiO_2-Al_2O_3-x possessed a higher yield of biogasoline upon

Table 4 Catalytic activity of SiO_2-Al_2O_3-x and SiO_2-Al_2O_3-x/NiMo towards hydrocracking of CPO

Catalysts	Conversion (%)	Yield (%)		
		Biogasoline (C_5-C_9)	Bio-aviation (C_{10}-C_{14})	Biodiesel (C_{15}-C_{22})
SiO_2-Al_2O_3-5	75.78	2.28	34.26	17.22
SiO_2-Al_2O_3-10	84.47	2.85	44.55	8.58
SiO_2-Al_2O_3-25	91.20	11.15	46.31	11.76
SiO_2-Al_2O_3-5/NiMo	92.99	18.13	62.92	1.70
SiO_2-Al_2O_3-10/NiMo	91.34	13.26	61.31	2.34
SiO_2-Al_2O_3-25/NiMo	91.73	18.47	58.00	2.00

introducing higher Al mass onto the support, presumably owing to the higher surface area and dominantly small pore diameter. It was reported that the fraction of gasoline was much more favorable to diffuse into a small pore than the larger fractions [16]. Upon NiMo loading, SiO_2-Al_2O_3-5/NiMo showed an increase in bio-aviation yield up to 62.92% along with higher biogasoline and decreased biodiesel yield compared to the unloaded SiO_2-Al_2O_3, which suppressed the formation of longer carbon chain biofuel due to the excessive cracking of longer carbon towards shorter carbon chain biofuels. The same trends were also observed with SiO_2-Al_2O_3-10/NiMo and SiO_2-Al_2O_3-10/NiMo with comparable catalytic activity for unloaded SiO_2-Al_2O_3-x, showing that SiO_2-Al_2O_3-x/NiMo promoted higher CPO yield and short-chain biofuels yield. Compared to SiO_2/Zr-KHF and SiO_2/ZrN-EDTA prepared by the template approach, the present catalysts showed comparable results with their counterparts under lower hydrocracking temperatures [11, 43]. Despite that controlling the Al mass in SiO_2/Al_2O_3-NiMo showed the textural and acidity features dependency. Future studies however must address the composition of the different phases and their oxidation state to completely understand the inherent features that eventually affect catalytic activity.

4 Conclusion

The effect of Al mass on the structure, acidity features, and CPO hydrocracking catalytic performance of SiO_2-Al_2O_3-x and SiO_2-Al_2O_3-x/NiMo were presented. Increasing Al mass led to an increase in the total acidity, surface area, and the amorphous feature of SiO_2/Al_2O_3. SiO_2/Al_2O_3-25 exhibited a better support, as evidenced by providing well-dispersed NiMo species. Hydrocracking test of the CPO showed that SiO_2-Al_2O_3-x/NiMo had higher CPO conversion and successfully formed higher dominant bio-aviation and biogasoline yields compared to unloaded SiO_2-Al_2O_3-x. These catalysts successfully suppressed the long carbon chain favoring the short carbon chain, showing good hydrocracking activity. Further analysis regarding the composition of different phases and their oxidation state must be considered to comprehend the properties of the catalysts and their catalytic process in CPO conversion.

Acknowledgement

The authors gratefully acknowledge to National research and innovation agency (BRIN), Indonesia, for funding this research through RIIM Batch III research grant contract No. 0256.03/UN9/SB3.LP2M.PT/2023.

References

[1] Barrón C., A. E., Melo-Banda, J. A., Dominguez E., J. M., Hernández M., E., Silva R., R., Reyes T., A. I., Meraz M., M. A. "Catalytic hydrocracking of vegetable oil for agrofuels production using Ni-Mo, Ni-W, Pt and TFA catalysts supported on SBA-15", Catalysis Today, 166(1), pp. 102–110, 2011. https://doi.org/10.1016/j.cattod.2011.01.026

[2] El-Deeb, Z. M., Aboutaleb, W. A., Mohamed, R. S., Dhmees, A. S., Ahmed, A. I. "Gasoline and diesel-like fuel production via hydrocrackin-g of hydrotreated tire pyrolytic oil over Ni-W/MCM-41 derived from blast furnace slag", Journal of the Energy Institute, 103, pp. 84–93, 2022. https://doi.org/10.1016/j.joei.2022.05.013

[3] Dujjanutat, P., Kaewkannetra, P. "Production of bio-hydrogenated kerosene by catalytic hydrocracking from refined bleached deodorised palm/ palm kernel oils", Renewable Energy, 147, pp. 464–472, 2020. https://doi.org/10.1016/j.renene.2019.09.015

[4] Šimáček, P., Kubička, D. "Hydrocracking of petroleum vacuum distillate containing rapeseed oil: Evaluation of diesel fuel", Fuel, 89(7), pp. 1508–1513, 2010. https://doi.org/10.1016/j.fuel.2009.09.029

[5] Saab, R., Polychronopoulou, K., Zheng, L., Kumar, S., Schiffer, A. "Synthesis and performance evaluation of hydrocracking catalysts: A review", Journal of Industrial and Engineering Chemistry, 89, pp. 83–103, 2020. https://doi.org/10.1016/j.jiec.2020.06.022

[6] Subsadsana, M., Ruangviriyachai, C. "Effect of NiW Modified HZSM-5 and HY Zeolites on Hydrocracking Conversion of Crude Palm Oil to Liquid Hydrocarbons", Oriental Journal of Chemistry, 32(2), pp. 839–844, 2016. https://doi.org/10.13005/ojc/320208

[7] Mirzayanti, Y. W., Kurniawansyah, F., Prayitno, D. H., Roesyadi, A. "Zn-Mo/HZSM-5 Catalyst for Gasoil Range Hydrocarbon Production by Catalytic Hydrocracking of Ceiba pentandra oil", Bulletin of Chemical Reaction Engineering & Catalysis, 13(1), pp. 136–143, 2018. https://doi.org/10.9767/bcrec.13.1.1508.136-143

[8] Kadarwati, S., Rahmawati, F., Eka Rahayu, P., Imam Supardi, K. "Kinetics and Mechanism of Ni/Zeolite-Catalyzed Hydrocracking of Palm Oil into Bio-Fuel", Indonesian Journal of Chemistry, 13(1), pp. 77–85, 2013. https://doi.org/10.22146/ijc.21330

[9] Zandonai, C. H., Yassue-Cordeiro, P. H., Castellã-Pergher, S. B., Scaliante, M. H. N. O., Fernandes-Machado, N. R. C. "Production of petroleum-like synthetic fuel by hydrocracking of crude soybean oil over ZSM5 zeolite-Improvement of catalyst lifetime by ion exchange", Fuel, 172, pp. 228–237, 2016. https://doi.org/10.1016/j.fuel.2015.12.059

[10] Alisha, G. D., Trisunaryanti, W., Syoufian, A., Larasati, S. "Synthesis of high stability Mo/SiO_2 catalyst utilizing Parangtritis beach sand for hydrocracking waste palm oil into biofuel", Biomass Conversion and Biorefinery, 13(12), pp. 11041–11055, 2023. https://doi.org/10.1007/s13399-021-02064-x

[11] Asri, W. R., Hasanudin, H., Wijaya, K. "Hydroconversion of Crude Palm Oil Over Highly Dispersed Porous Silica Modified Zirconium Nitride: Effect of EDTA and KHF Template", Silicon, 16(1), pp. 83–97, 2024.
https://doi.org/10.1007/s12633-023-02659-1

[12] Allwar, A., Maulina, R., Julianto, T. S., Widyaningtyas, A. A. "Hydrocracking of Crude Palm Oil over Bimetallic Oxide NiO-CdO/biochar Catalyst", Bulletin of Chemical Reaction Engineering & Catalysis, 17(2), pp. 476–485, 2022.
https://doi.org/10.9767/bcrec.17.2.14074.476-485

[13] Mampuru, M. B., Nkazi, D. B., Mukaya, H. E. "Hydrocracking of waste cooking oil into biogasoline in the presence of a bi-functional Ni-Mo/alumina catalyst", Energy Sources, Part A: Recovery, Utilization and Environmental Effects, 42(20), pp. 2564–2575, 2020.
https://doi.org/10.1080/15567036.2019.1610527

[14] Anand, M., Farooqui, S. A., Kumar, R., Joshi, R., Kumar, R., Sibi, M. G., Singh, H., Sinha, A. K. "Optimizing renewable oil hydrocracking conditions for aviation bio-kerosene production", Fuel Processing Technology, 151, pp. 50–58, 2016.
https://doi.org/10.1016/j.fuproc.2016.05.028

[15] Subsadsana, M., Sansuk, S., Ruangviriyachai, C. "Enhanced liquid biofuel production from crude palm oil over synthesized NiMoW-ZSM-5/MCM-41 catalyst", Energy Sources, Part A: Recovery, Utilization, and Environmental Effects, 40(2), pp. 237–243, 2018.
https://doi.org/10.1080/15567036.2017.1411992

[16] Alisha, G. D., Trisunaryanti, W., Syoufian, A. "Hydrocracking of Waste Palm Cooking Oil into Hydrocarbon Compounds over Mo Catalyst Impregnated on SBA-15", Silicon, 14(5), pp. 2309–2315, 2022.
https://doi.org/10.1007/s12633-021-01035-1

[17] Žula, M., Grilc, M., Likozar, B. "Hydrocracking, hydrogenation and hydro-deoxygenation of fatty acids, esters and glycerides: Mechanisms, kinetics and transport phenomena", Chemical Engineering Journal, 444, 136564, 2022.
https://doi.org/10.1016/j.cej.2022.136564

[18] Nadia, A., Wijaya, K., Falah, I. I., Sudiono, S., Budiman, A. "Self-regeneration of Monodisperse Hierarchical Porous NiMo/Silica Catalyst Induced by $NaHCO_3$ for Biofuel Production", Waste and Biomass Valorization, 13(4), pp. 2335–2347, 2022.
https://doi.org/10.1007/s12649-021-01634-4

[19] Ishihara, A., Fukui, N., Nasu, H., Hashimoto, T. "Hydrocracking of soybean oil using zeolite-alumina composite supported NiMo catalysts", Fuel, 134, pp. 611–617, 2014.
https://doi.org/10.1016/j.fuel.2014.06.004

[20] Jafarian, S., Tavasoli, A., Nikkhah, H. "Catalytic hydrotreating of pyro-oil derived from green microalgae spirulina the (*Arthrospira*) plantensis over NiMo catalysts impregnated over a novel hybrid support", International Journal of Hydrogen Energy, 44(36), pp. 19855–19867, 2019.
https://doi.org/10.1016/j.ijhydene.2019.05.182

[21] Yang, J. K., Zuo, T. J., Lu, Y. Y., Zeng, W. S., Lu, J. Y. "Catalytic performance of NiMo/Al_2O_3-USY in the hydrocracking of low-temperature coal tar", Journal of Fuel Chemistry and Technology, 47(9), pp. 1053–1066, 2019.
https://doi.org/10.1016/s1872-5813(19)30043-x

[22] Xu, J., Huang, T., Fan, Y. "Highly efficient NiMo/SiO_2-Al_2O_3 hydrodesulfurization catalyst prepared from gemini surfactant-dispersed Mo precursor", Applied Catalysis B: Environmental, 203, pp. 839–850, 2017.
https://doi.org/10.1016/j.apcatb.2016.10.078

[23] Li, M., Ihli, J., Verheijen, M. A., Holler, M., Guizar-Sicairos, M., van Bokhoven, J. A., Hensen, E. J. M., Weber, T. "Alumina-Supported NiMo Hydrotreating Catalysts─Aspects of 3D Structure, Synthesis, and Activity", The Journal of Physical Chemistry C, 126(43), pp. 18536–18549, 2022.
https://doi.org/10.1021/acs.jpcc.2c05927

[24] Kaluža, L., Palcheva, R., Spojakina, A., Jirátová, K., Tyuliev, G. "Hydrodesulfurization NiMo catalysts supported on Co, Ni and B modified Al_2O_3 from Anderson heteropolymolybdates", Procedia Engineering, 42, pp. 873–884, 2012.
https://doi.org/10.1016/j.proeng.2012.07.480

[25] Aneu, A., Wijaya, K., Syoufian, A. "Silica-Based Solid Acid Catalyst with Different Concentration of H_2SO_4 and Calcination Temperature: Preparation and Characterization", Silicon, 13(7), pp. 2265–2270, 2021.
https://doi.org/10.1007/s12633-020-00741-6

[26] Srihanun, N., Dujjanutat, P., Muanruksa, P., Kaewekannetra, P. "Biofuels of Green Diesel–Kerosene–Gasoline Production from Palm Oil: Effect of Palladium Cooperated with Second Metal on Hydrocracking Reaction", Catalysts, 10(2), 241, 2020.
https://doi.org/10.3390/catal10020241

[27] Leyva, C., Ancheyta, J., Travert, A., Maugé, F., Mariey, L., Ramírez, J., Rana, M. S. "Activity and surface properties of NiMo/SiO_2–Al_2O_3 catalysts for hydroprocessing of heavy oils", Applied Catalysis A: General, 425–426, pp. 1–12, 2012.
https://doi.org/10.1016/j.apcata.2012.02.033

[28] Tavasoli, A., Taghizadeh Yusefabad, E., Zamani, Y. "Hydrocracking process and kinetic equation: Effect of the fluoride on the performance of the Ni-Mo catalyst", Energy Science & Engineering, 9(8), pp. 1103–1114, 2021.
https://doi.org/10.1002/ese3.876

[29] Hao, F., Zhong, J., Liu, P.-L., You, K.-Y., Luo, H.-A. "Amorphous SiO_2-Al_2O_3 supported Co_3O_4 and its catalytic properties in cyclohexane nitrosation to ε-caprolactam: Influences of preparation conditions", Journal of Molecular Catalysis A: Chemical, 363–364, pp. 41–48, 2012.
https://doi.org/10.1016/j.molcata.2012.05.014

[30] Lee, J. S., Kim, H. S., Park, N.-K., Lee, T. J., Kang, M. "Low temperature synthesis of α-alumina from aluminum hydroxide hydrothermally synthesized using [Al(C_2O_4)x(OH)y] complexes", Chemical Engineering Journal, 230, pp. 351–360, 2013.
https://doi.org/10.1016/j.cej.2013.06.099

[31] Liang, Y., Shi, G., Jin, K. "Promotion Effect of Al_2O_3 on Pt–WO_x/SiO_2 Catalysts for Selective Hydrogenolysis of Bioglycerol to 1,3-Propanediol in Liquid Phase", Catalysis Letters, 150(8), pp. 2365–2376, 2020.
https://doi.org/10.1007/s10562-020-03140-z

[32] Priecel, P., Kubička, D., Vázquez-Zavala, A., Antonio de los Reyes, J., Pouzar, M., Čapek, L. "Alternative Preparation of Improved NiMo-Alumina Deoxygenation Catalysts", Frontiers in Chemistry, 8, 216, 2020.
https://doi.org/10.3389/fchem.2020.00216

[33] Hamidi, R., Khoshbin, R., Karimzadeh, R. "A new approach for synthesis of well-crystallized Y zeolite from bentonite and rice husk ash used in Ni-Mo/Al_2O_3-Y hybrid nanocatalyst for hydrocracking of heavy oil", Advanced Powder Technology, 32(2), pp. 524–534, 2021.
https://doi.org/10.1016/j.apt.2020.12.029

[34] Li, J., Li, P., Li, J., Tian, Z., Yu, F. "Highly-Dispersed Ni-NiO Nanoparticles Anchored on an SiO_2 Support for an Enhanced CO Methanation Performance", Catalysts, 9(6), 506, 2019.
https://doi.org/10.3390/catal9060506

[35] Badoga, S., Mouli, K. C., Soni, K. K., Dalai, A. K., Adjaye, J. "Beneficial influence of EDTA on the structure and catalytic properties of sulfided NiMo/SBA-15 catalysts for hydrotreating of light gas oil", Applied Catalysis B: Environmental, 125, pp. 67–84, 2012.
https://doi.org/10.1016/j.apcatb.2012.05.015

[36] Ayandiran, A. A., Boahene, P. E., Nanda, S., Dalai, A. K., Hu, Y. "Hydroprocessing of oleic acid for the production of aviation turbine fuel range hydrocarbons over bimetallic Fe-Cu/SiO_2-Al_2O_3 catalysts promoted by Sn, Ti and Zr", Molecular Catalysis, 523, 111358, 2022.
https://doi.org/10.1016/j.mcat.2020.111358

[37] Zitouni, A., Bachir, R., Bendedouche, W., Bedrane, S. "Production of bio-jet fuel range hydrocarbons from catalytic HDO of biobased difurfurilydene acetone over Ni/SiO_2-ZrO_2 catalysts", Fuel, 297, 120783, 2021.
https://doi.org/10.1016/j.fuel.2021.120783

[38] Escalona, G., Rai, A., Betancourt, P., Sinha, A. K. "Selective poly-aromatics saturation and ring opening during hydroprocessing of light cycle oil over sulfided Ni-Mo/SiO_2-Al_2O_3 catalyst", Fuel, 219, pp. 270–278, 2018.
https://doi.org/10.1016/j.fuel.2018.01.134

[39] Asri, W. R., Hasanudin, H., Wijaya, K. "Highly Active Mesoporous Zirconium Nitride Immobilized on SiO_2 Synthesized by Complex-Assisted Method with EDTA and KHP for Catalytic Hydroconversion of Crude Palm Oil", Catalysis Surveys from Asia, 28(1), pp. 74–87, 2024.
https://doi.org/10.1007/s10563-023-09413-y

[40] Papageridis, K. N., Charisiou, N. D., Douvartzides, S. L., Sebastian, V., Hinder, S. J., Baker, M. A., AlKhoori, S., Polychronopoulou, K., Goula, M. A. "Effect of operating parameters on the selective catalytic deoxygenation of palm oil to produce renewable diesel over Ni supported on Al_2O_3, ZrO_2 and SiO_2 catalysts", Fuel Processing Technology, 209, 106547, 2020.
https://doi.org/10.1016/j.fuproc.2020.106547

[41] Liu, Q., Li, J., Zhao, Z., Gao, M., Kong, L., Liu, J., Wei, Y. "Synthesis, characterization, and catalytic performances of potassium-modified molybdenum-incorporated KIT-6 mesoporous silica catalysts for the selective oxidation of propane to acrolein", Journal of Catalysis, 344, pp. 38–52, 2016.
https://doi.org/10.1016/j.jcat.2016.08.014

[42] Malins, K. "Synthesis of renewable hydrocarbons from vegetable oil feedstock by hydrotreatment over selective sulfur-free SiO_2-Al_2O_3 supported monometallic Pd, Pt, Ru, Ni, Mo and bimetallic NiMo catalysts", Fuel, 285, 119129, 2021.
https://doi.org/10.1016/j.fuel.2020.119129

[43] Hasanudin, H., Asri, W. R., Mara, A., Al Muttaqii, M., Maryana, R., Rinaldi, N., Sagadevan, S., Zhang, Q., Fanani, Z., Hadiah, F. "Enhancement of Catalytic Activity on Crude Palm Oil Hydrocracking over SiO_2/Zr Assisted with Potassium Hydrogen Phthalate", ACS Omega, 8(23), pp. 20858–20868, 2023.
https://doi.org/10.1021/acsomega.3c01569

[44] Vandevyvere, T., Sabbe, M. K., Mendes, P. S. F., Thybaut, J. W., Lauwaert, J. "NiCu-based catalysts for the low-temperature hydrodeoxygenation of anisole: Effect of the metal ratio on SiO_2 and γ-Al_2O_3 supports", Green Carbon, 1(2), pp. 170–184, 2023.
https://doi.org/10.1016/j.greenca.2023.10.001

[45] Leyva, C., Ancheyta, J., Mariey, L., Travert, A., Maugé, F. "Characterization study of NiMo/SiO_2-Al_2O_3 spent hydroprocessing catalysts for heavy oils", Catalysis Today, 220–222, pp. 89–96, 2014.
https://doi.org/10.1016/j.cattod.2013.10.007